ARTICLE

Electrochemical gating for single-molecule electronics with hybrid Au|graphene contacts

Received 00th January 20xx,
Accepted 00th January 20xx

DOI: 10.1039/x0xx00000x

Shuhui Tao,[a,b] Qian Zhang,[a,b] Andrea Vezzoli,[b] Cezhou Zhao,[c] Chun Zhao,[c] Simon J. Higgins,[b] A. Smogunov,[d] Yannick J. Dappe,*[d] Richard J. Nichols[b] and Li Yang*[a,b]

The single-molecular conductance of a redox active viologen molecular bridge between Au|graphene electrodes has been studied in an electrochemical gating configuration in an ionic liquid medium. A clear "off-on-off" conductance switching behaviour has been achieved through gating of the redox state when the electrochemical potential is swept. The Au|viologen|graphene junctions show single-molecule conductance maxima centred close to the equilibrium redox potentials for both reduction steps. The peak conductance of Au|viologen|graphene junctions during the first reduction is significantly higher than that of previously measured Au|viologen|Au junctions. This shows that even though the central viologen moiety is not directly linked to the enclosing electrodes, substituting one gold contact for a graphene one nevertheless has a significant impact on junction conductance values. The experimental data was compared against two theoretical models, namely a phase coherent tunnelling and an incoherent "hopping" model. The former is a simple gating monoelectronic model within density functional theory (DFT) which discloses the charge state evolution of the molecule with electrode potential. The latter model is the collective Kuznetsov Ulstrup model for 2-step sequential charge transport through the redox centre in the adiabatic limit. The comparison of both models to the experimental data is discussed for the first time. This work opens perspectives for graphene-based molecular transistors with more effective gating and fundamental understanding of electrochemical electron transfer at the single molecular level.

Introduction

The electrochemical scanning tunnelling microscope (EC-STM) is a powerful tool for studying charge transport through single molecules at the electrode-electrolyte interface. As the electrode potential is tuned, the current between the scanning tunnelling microscope (STM) tip and the electrode surface can be modulated. Here, the electrolyte can be referred as the "liquid gate", and the process has been termed a "single molecule electrochemical gating". Using analogies with conventional field effect transistors, the STM tip and the electrode surface are then referred to as source and drain, and this source-drain (bias) voltage can be separately controlled alongside the gating potential between each working electrode and a reference electrode. There are now diverse examples of redox active molecular bridges studied using such methodology including viologens,[1-11] (anthra)quinones,[12-14] tetrathiafulvalene and benzodifuran derivatives,[6, 15, 16] short conducting oligomers,[17-21] metallo-organic compounds[22-24] and perylene or naphthalene tetracarboxylic diimides.[25-32] These multifarious redox active single molecular wires have been studied under diverse electrochemical conditions.

A "viologen" molecular wire with thiol terminated group linked ("wired") to two gold electrodes was the first electrochemical redox system to be studied in wired single molecular junctions.[1] Since then viologens have been a popular model system for fundamental studies using single molecular electrochemical STM methods.[1-11] The interest in "viologen" systems lies in the redox reaction of the V^{2+} moiety which is electrochemically reduced to its radical cation form $V^{+\cdot}$ in its first reduction step. Under electrochemical control, the redox centre of viologens can be reduced and oxidized reversibly to produce different conductance states. The conductance behaviour of Au|viologen|Au system has been reported in aqueous media[5] and ionic liquid (IL) media.[10] It was found that the conductance of Au|viologen|Au features a monotonic sigmoidal increase upon making the potential more negative in aqueous media. By contrast the same Au|viologen|Au system showed a "bell shape" conductance variation in ionic liquid media. These data have been interpreted in terms of the two-step electron transfer mechanism proposed by Kuznetzov and Ulstrup (see [33] and references therein), an alternative "soft gating" model was given for the sigmodal curves in aqueous electrolytes.[10, 34] In the former case, electrons transfer between the two gold contacts through the redox active viologen moiety. Due to strong electronic coupling between the charge donor and acceptor in the adiabatic limit, multiple electronic

[a] Department of Chemistry, Xi'an-Jiaotong Liverpool University, Suzhou, 215123, China.
[b] Department of Chemistry, University of Liverpool, Liverpool, L69 7ZD, UK.
[c] C. Department of Electrical and Electronic Engineering, Xi'an-Jiaotong Liverpool University, Suzhou, 215123, China.
[d] SPEC, CEA, CNRS, Université Paris-Saclay, CEA Saclay 91191 Gif-sur-Yvette Cedex, France.

† Footnotes relating to the title and/or authors should appear here.
Electronic Supplementary Information (ESI) available: [details of any supplementary information available should be included here]. See DOI: 10.1039/x0xx00000x

transitions take place during passage of the electronic energy level through a region near the Fermi level of the electrode. A boost of the junction current at the redox switching potential is obtained. For the viologen system in aqueous electrolyte, an alternative model has been used to rationalize the slow rise in conductance with overpotential. This "soft gating" model for this slow rise in conductance was also developed by Kuznetsov and Ulstrup, is a superexchange tunnelling mechanism in which the molecular bridge exhibits large configuration fluctuations, which promote level alignment conducive to effective tunnelling through the bridge. The viologen bridge is not reduced as the potential is moved across the equilibrium potential but nevertheless the favourable configurations boost the tunnelling current giving an electrolyte gating effect.[5]

Despite significant progress, investigating different redox molecules, very few previous attempts have been made to broaden the range of electrodes studied. In the field of single molecule electronics, both for electrochemical and non-electrochemical (2-terminal) studies, the most commonly used contact is still gold, since gold electrodes offers good chemical stability, straightforward contact fabricability and are generally free from oxide under ambient conditions. Moreover, gold can form sufficiently strong metal-molecule covalent bonding such as Au-S, Au-NH, and Au-COO,[35-37] providing a model metal-molecule contact for molecular electronics. However, limitations of gold electrodes for possible future molecular devices are also apparent, including the high cost and their non-compatibility with complementary metal-oxide-semiconductor (CMOS) technologies. In 2015, Brooke and co-workers used a scanning tunnelling microscope break junction (STM-BJ) technique to produce 4,4'-bipyridine (44BP) single molecule junctions with Ni and Au contacts. A key observation was that the resulting conductance of the Ni-44BP-Ni electrochemical transistors is significantly higher than the analogous Au-based devices.[38] The use of other novel electrodes promises new platforms for molecular device fabrication. Indeed, new phenomena have been reported for molecular devices using indium–tin oxide (ITO),[39] carbon-based materials,[40-44] and semiconductors such as gallium arsenide (GaAs),[45,46] or silicon as contacting electrodes.[47] In our previous studies, it was found that using Au|graphene electrodes and appropriate anchoring groups such as amine or thiol could lead to a much lower decay constant (β) even for aliphatic molecular bridges.[41,42]

In the present study we examine, for the first time, charge transport and electrochemical switching in Au|redox molecule|graphene junctions in ionic liquids and compare the conductance with data from the counterpart Au|Au devices. The target molecule chosen is an alkyl chain modified viologen molecular wire (6V6) terminated with thiol anchoring groups at each end. Ionic liquids are being used successfully in a growing number of molecular electronics and single molecule electrochemical STM studies.[10, 16, 31, 48-52] The use of ionic liquid electrolytes, rather than traditional organic electrolytes or aqueous media, is attractive due to their chemical tunability, low vapour pressure, and large electrochemical window.[53-56] Osorio et al.[10] reported that in electrochemically gated junctions, ILs are more effective than aqueous electrolytes in coupling the molecule to the gate electrode.

Results and discussion

The redox behaviour of 6V6 with a graphene working electrode was examined in the ionic liquid 1-butyl-3-methylimidazolium triflate (BMIM-OTf) solution using cyclic voltammetry (CV). The substrates used in our experiments are a few layers of graphene, as confirmed by Raman spectroscopy in the supporting information (Figure S3a). For these CV experiments 5 mM of 6V6 was dissolved in the BMIM-OTf, So the CV response corresponds to the diffusion controlled reduction of the solution species. 6V6 undergoes a two-electron transfer process, namely $V^{2+} + e^- \rightarrow V^{+\bullet}$ and $V^{+\bullet} + e^- \rightarrow V^0$, with V = viologen, as shown in Figure 1a. With the larger electrochemical window in BMIM-OTf, both electron transfer waves are apparent in the CV. The peak-to-peak separation of first redox wave ($V^{2+} + e^- \rightarrow V^{+\bullet}$) is at around 145 mV, while the second wave is observed at 180 mV. In the case of both waves the cathodic and corresponding anodic peaks do not line up at the same potential, as would be expected for an ideal reversible redox switching of a surface attached redox group. The non-ideality of the CV waves could arise from quasi-reversibility, structural changes in the SAM during reduction and kinetic or structural effects associated with the insertion or removal of counterions associated with charge balance. With these limitations in mind, we take the central point between each respective CV wave as an approximation of the equilibrium redox potential, which is in turn used in the modelling presented latter. It is worth noting that this measured CV (as shown in Figure 1b) shows a sloped baseline, particularly apparent at the second redox wave ($V^{+\bullet} + e^- \rightarrow V^0$). This slope may be due to a minute amount of residual water in the IL or a small amount of O_2. Using the Randles-Ševčík equation, the diffusion coefficient based on the $V^{2+} + e^- \rightarrow V^{+\bullet}$ reduction in BMIM-OTf was calculated as $D = 2.8 \times 10^{-8} cm^2\ s^{-1}$.

We measured the conductance value of Au|6V6|graphene junctions using the EC-STM *I*(s) technique. For each of the molecular junction formed at a given electrode potential, more than 300 *I*(s) curves featuring plateaus were recorded. These were then used to construct the conductance 1D histogram as shown in Figure 2a. For each of the 1D conductance histograms a clear peak is observed, indicating the most probable conductance value of the molecular junctions at that given electrode potential.

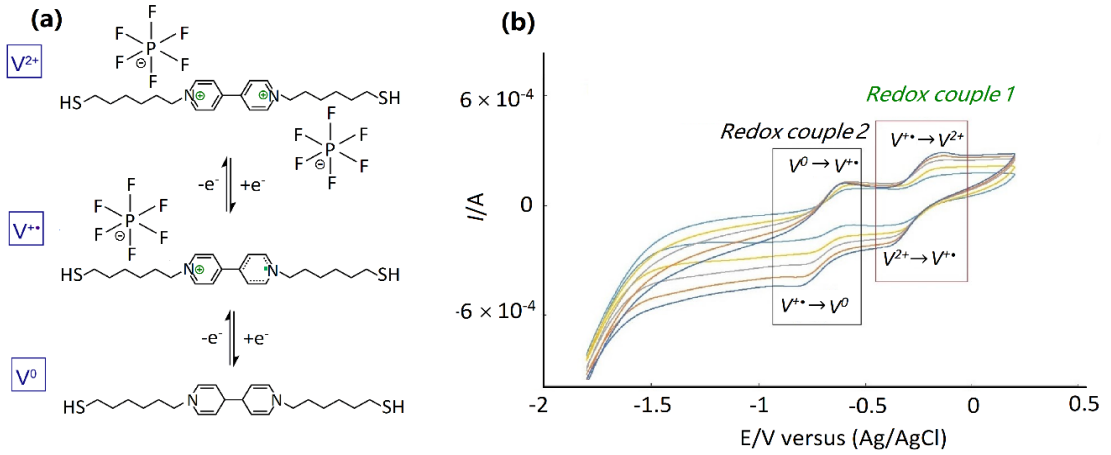

Figure 1: (a) The viologen based molecule (6V6), undergoes the two-step redox reaction of $V^{2+} + e^- \rightarrow V^{+\bullet}$, and $V^{+\bullet} + e^- \rightarrow V^0$. (b) Cyclic voltammograms recorded for the reduction of 6V6 (5 mM) in BMIM-OTf. The system was referenced against Ag/AgCl reference electrode. The CVs were run at between 0.2 V/s and 1 V/s with a graphene working electrode, Pt counter electrode and Ag/AgCl reference electrode. The right redox couple corresponds to the one-electron reduction of the bipyridinium redox centre (V^{2+}) to the radical anion ($V^{+\bullet}$), while the second redox couple corresponds to the electron transfer between ($V^{+\bullet}$) and (V^0).

When the electrochemical single molecule conductance data (taken from the histogram peaks of current plateau values) is plotted for fourteen different electrode potentials two bell-shaped profiles are observed. Figure 2b shows this single molecule conductance data for Au|6V6|graphene over the range of electrode potentials with a cyclic voltammogram superimposed on the same potential axis. The error bars were calculated from the full width half maximum (FWHM) of the gaussian peak fitting of the 1D conductance histogram values. A conductance maximum of 5.9 nS is apparent, and this occurs at around the redox equilibrium potential for the first redox reaction, $V^{2+} + e^- \rightarrow V^{+\bullet}$. As the electrode potential is swept from positive to negative electrode values through this first redox process the system follows a "off-on-off" conductance switching profile.[50] As noted above the CV peaks display irreversibility, but as an approximation we have taken the centre point between the peaks as an approximation of the equilibrium redox potential for $V^{2+}|V^{+\cdot}$ redox switching for the first wave and $V^{+\cdot}|V^0$ switching for the more cathodic redox wave. This behaviour with a maximum molecular conductance close to the $V^{2+}|V^{+\cdot}$ reversible potential is similar to the well-known Au|Au system (shown in Figure S9). These data show that asymmetric Au|graphene electrode contacting offers highly effective gating in ionic liquid. The conductance of Au|6V6|graphene molecular junctions changes from 5.9 nS ("on" state) at -0.25 V to 1.7 nS ("off") at -0.95 V, which corresponds to a factor of 3.5 between "on" and "off". In the case of the Au|6V6|Au system in ionic liquid a comparable "on"/"off" ratio of 3.7 is observed.[10] The peak conductance of Au|6V6|graphene molecular junctions (5.9 nS) is however higher than that of Au|6V6|Au junctions (1.5 nS) in ionic liquid. This higher conductance of molecular junction with hybrid

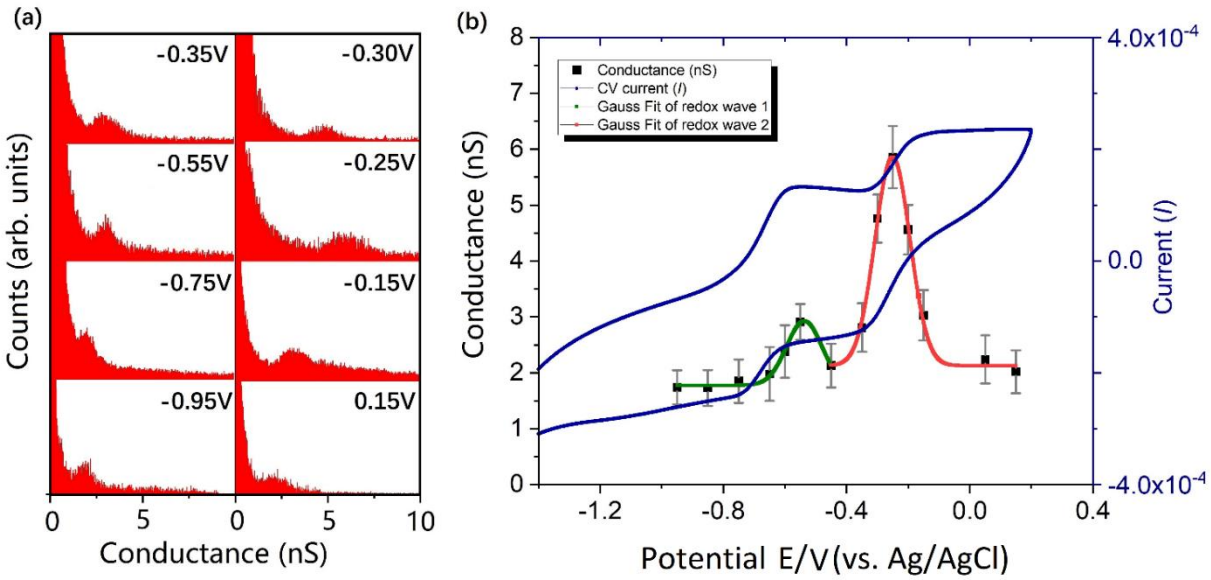

Figure 2: (a) One-dimensional (1D) histogram representations of Au|6V6|graphene conductance behaviour recorded at the electrode potentials of -0.95 V, -0.75 V, -0.55 V, -0.35 V, -0.30 V, -0.25 V, -0.15V, 0.15 V (versus Ag/AgCl). (b) The peak conductance of Au|6V6|graphene junctions against the sample electrode potential, overlaid with a cyclic voltammogram (blue line) of 6V6 in BMIM-OTf.

Au|graphene electrode contacting is in agreement with our previous non-electrochemical (2-terminal) STM studies.[41-43] This can be attributed to the weak van der Waals coupling with the graphene electrode, where the molecular electronic levels are not hybridized with the graphene electronic level. Hence, no broadening of the molecular electronic level is observed which leads to sharper molecular resonances. In addition, there is a less prominent peak in the molecular conductance versus electrode potential plot at -0.55 V in Figure 2b. This conductance increase could be considered as a response to the second redox reaction $V^{+\bullet}|V^0$, which has not been previously observed. These data show the first example of electrochemical gating of single molecule conductance with a graphene substrate electrode.

These experimental data for the gating of Au|6V6|graphene junctions have been considered theoretically against two different mechanisms, namely phase coherent tunnelling and sequential 2-step electron transfer. In both cases the influence of the electrode potential on the evolution of the junction conductance is modelled. In the case of phase coherent tunnelling the gating is modelled by consideration of the evolution of the charge state of the viologen moiety within the molecular bridge. Here density functional theory (DFT) computations have been performed for the junction with different molecular charges (by adding or removing electrons to the full system and then proceeding to the electronic self-consistency). This approach is similar to previous calculations where counter ions have been added to the system in order to tune the molecular charge.[57] The main objective is to simulate the experimental molecular gating by changing the charge state of the molecule in a self-consistent manner, and to deduce the corresponding electronic transmissions.[58-60] The molecular levels are shifted due to the gating and the resonance is obtained when a molecular level crosses the Fermi level. In Figure 2, we can observe two conductance peaks which are related to the two redox states observed in the CV measurement. Also, the maxima of these conductance peaks obviously correspond to the respective molecular resonances, when a shifted molecular level is located at the Fermi level. The unit cell used for the calculations, namely the molecule between the gold and graphene electrode, plus the two PF_6^- ions, is represented in Figure 3a. The orientation of 6V6 molecule span to the junction is confirmed by comparing the break-off distance (More detailed calculation of the break-off distance can be found in SI and Figure S6) against the length of fully extended 6V6 molecule (Figure S7). The corresponding transmission curves calculated for molecular charges ranging from -2.71 to -1.71 electrons (*i.e.* 2.71 to 1.71 electrons removed from the molecules, as a result after self-consistency calculations of adding/removing the necessary electrons to the whole system to obtain the corresponding molecular level shift) are represented in Figure 3b. Note that the equilibrium state of the system, without any gating, corresponds to a molecular charge -2.13 electrons (2.13 electrons removed from the molecule to the electrodes), namely close to the V^{2+} state of the molecular bridge. Here there is a small difference in the charge states of the molecular bridge calculated using DFT with the recognised viologen redox states observed in CV measurements. It is noted here that in the CVs the peaks are related to reduction/oxidation of SAMs in aqueous electrolytes between defined redox state, while DFT does not include the medium, details of the SAM structure or counterions from the electrolyte (*i.e.* DFT modelling is for the *in vacuo* situation). This rationalises the small charge difference in the molecular bridge calculated using DFT with respect to the 2^+ state, for example.

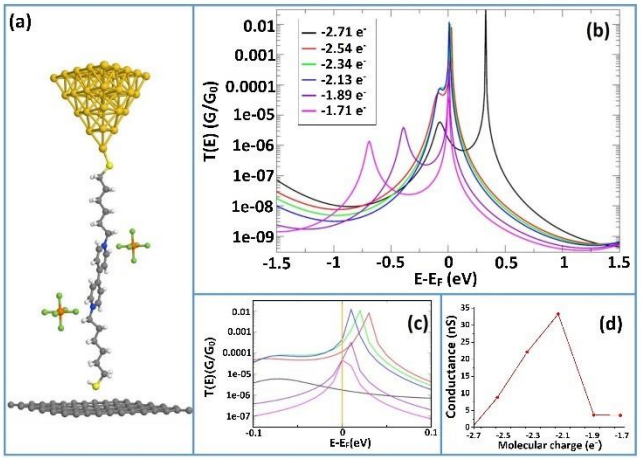

Figure 3: (a) Atomistic representation of the molecular junction and its two PF_6^- ions used for the DFT calculations. (b) Corresponding calculated electronic transmission curves for different molecular charge states. (c) A zoom of the transmissions near the Fermi level, showing the evolution of the conductance with the molecular charge, where the legend is same as Figure 3b. (d) Evolution of the calculated conductance as a function of the molecular charge.

As a main feature, one can observe a strong resonance near the Fermi level for almost all the transmission curves calculated with different molecular charge states. This is related to the evolution of the HOMO level of the molecule with the removal of about two electrons from the bipyridine core, reaching a full resonance at around -1.5 electrons, near the V^{2+} state. However, with the charging of the molecule, from -2.71 electrons to -1.71 electrons (gaining one electron in the whole range), a shift of the transmission spectra towards negative energies is seen (Figure 3c). This situation is similar to what happens in a semiconductor -based transistor when applying a gate potential.[33] Hence, the application of a gate potential in our experiments modifies the molecular charge around the V^{2+} state, and the measured conductance will be maximum at that resonance.

The evolution of the calculated conductance as a function of the molecular charge is represented in Figure 3d. A reduction of the molecular charge corresponds experimentally here to the application of a negative gating potential, transferring electrons to the molecule. Experimentally, the highest conductance is observed at the redox equilibrium state between V^{2+} and V^{+} as a mix of both populations. Further charging of the molecule would yields a second resonance, related to the $V^{+\cdot}$ state, where the charge state of the molecule would be around -1 electron.

Obviously, a fully quantitative comparison between DFT and experimental results is difficult to obtain as a result of normal

approximations implicit to the method. Nevertheless, DFT still represents a correct approximation of the electronic structure of a realistic system, which is hardly reachable using a model Hamiltonian. Also, the conductance is extracted from calculations in the neighbourhood of mathematical resonances, leading to high maxima, which are of course not observed under real experimental conditions. Consequently, the theoretical gating curve presents a higher maximum than what is observed experimentally. However, the physical behaviour of the molecular junction is well captured by the gating model we use here and the main message remains that the bell curve experimentally observed is related to a tuning of the charge state of the molecule.

Comparison with similar computations for the gold-gold junctions leads to analogous results. This correlates with the similarity of the experimental data for Au|6V6|Graphene and Au|6V6|Au junctions (see Figure S9b). The main differences lie in the initial charge state of the molecule that drives the amplitude of the gate potential to be applied to reach the maximum of resonance. Regarding the similar conductance values, this can be attributed to the decoupling of the active molecular part with the alkyl linker chains. These relatively poor conducting chains can be thought of as decoupling the viologen redox centre from the enclosing contacts thereby reducing the role of the electrodes. This feature is illustrated for the Au|6V6|Au junction through the isoelectronic density of states calculation shown in Figure S11. The electronic density is localized near the redox active part, with no contribution along the alkyl chains.

We next turn to modelling the data to sequential 2-step electron transfer in the adiabatic limit. This mechanism is described in the introduction. An analytical representation of this model is given below, and this can be used to numerically fit the experimental data:[33]

$$j_{enhanced} \approx j_0 \exp\left(-\lambda/4kT\right) \frac{\exp\left(e|V_{bias}|/4kT\right)}{cosh\left(\frac{e(0.5-\gamma)V_{bias} - e\xi\eta}{2kT}\right)}$$

This equation describes the enhanced current (j_{enhanced}) through the molecular junction as a function of the electrochemical overpotential (η) and further details can be found in [33] and references therein. The terms in this equation are the reorganization energies (λ), the bias voltage (V_{bias}), the fraction of the electrode potential (ξ) and the bias voltage (γ) experienced at the redox centre, the charge on an electron (e), Boltzmann's constant (k) and the absolute temperature (T).[61] An expression for the preexponential factor is:[33]

$$j_0 = en\omega_{eff}/2\pi$$

With[33]

$$n \approx eV_{bias}\left(\frac{1}{2\kappa_L\rho_L} + \frac{1}{\kappa_R\rho_R}\right)^{-1}$$

The two contacting electrodes are labelled here as left (L) and right (R). The terms in the two latter equations are the electron transmission coefficient (κ) and the electronic density of states (ρ) in the electrodes close to the Fermi level. ω_{eff} refers to the effective nuclear vibrational frequencies.

Use of this equation requires values for κ, ρ and ω_{eff} to be judiciously selected. Since the modelling is in the adiabatic limit the electron transmission coefficients are taken to be unity. The electronic density of states in the electrodes close to the Fermi level are computed at first principle level using DFT. DOS calculation have been made for gold and graphene electrodes. In the case of graphene there is a small p doping for the graphene contact, as the Dirac point is located at around 0.4 eV above the Fermi level. Numerical values of 10.97 eV^{-1} for the DOS of gold and 0.86 eV^{-1} for the DOS of graphene are obtained, giving approximately a factor of around ten differences between the two different electrode materials. The term ω_{eff} is trickier since we have no method for directly experimentally evaluating this or numerically calculating in from first principal computations. Previous work has used $\omega_{eff}/2\pi = \sim 10^{11}$ to 10^{12} Hz.[62] Such frequencies might align with low frequency nuclear modes. Given the uncertainty in the choosing an optimal numerical value for ω_{eff} two limits are chosen here, a lower frequency value (200 cm^{-1} or 6 × 10^{12} Hz) and a higher value (1000 cm^{-1}) which might be more representative of higher frequency modes associated with the viologen rings.

Fitting of the experimental single molecule data to the KU model is shown in Figure 4. This plots enhanced junction current, which is the current at the given electrode potential above the junction current which flows at a potential away from both maxima. This baseline current, taken here from the experimental junction current value at -0.95 V, is subtracted to give the enhanced current. Fitting is achieved for both the first and second reduction waves. For the purpose of the fitting, the maxima are taken to fall at the respective reversible potentials, which is reasonable since the mid-points of the CV waves in Figure 2b falls at values close to respective conductance maxima. The fit in Figure 4 is for the chosen higher frequency value for ω_{eff} (1000 cm^{-1}) and the fitting parameters can be found in Table 1 in the supporting information. This yields numerical fit values of reorganisation energies for the first and second reduction of 0.27 and 0.4 eV, respective. Taking the lower ω_{eff} (200 cm^{-1}) gives values of 0.1 eV for the first and 0.24 eV for the second reduction. In all cases, for the purpose of the fitting, the maxima are taken to fall at the respective reversible potentials, with the fraction of the electrode potential experienced at the redox sites set to unity. This attests to the very efficient electrochemical gating in the ionic liquid which has been previously discussed.[10,50] Note that for this model the smaller single molecule conductance enhancement for the second reduction of the viologen is a result of a significantly higher reorganisation energy for this process compared to the first reduction. It is not unreasonable that the first and second reduction processes present different reorganisation energies since they result in different electronic structural changes in the viologen moiety. A note of caution is added here regarding quantitative fitting, in that the model is formulated for small overpotentials and small bias voltages such that $e\eta$ and eV_{bias} are significantly smaller than the inferred reorganisation

energies. In our measurements eV_{bias} (200 meV) is somewhat smaller than the inferred reorganisation energies for ω_{eff} = 1000 cm^{-1}. However, it is experimentally not possible to measure such data at the very low bias voltage values which might be theoretically desired, since the junction current would be too low to experimentally determine at very low bias values.

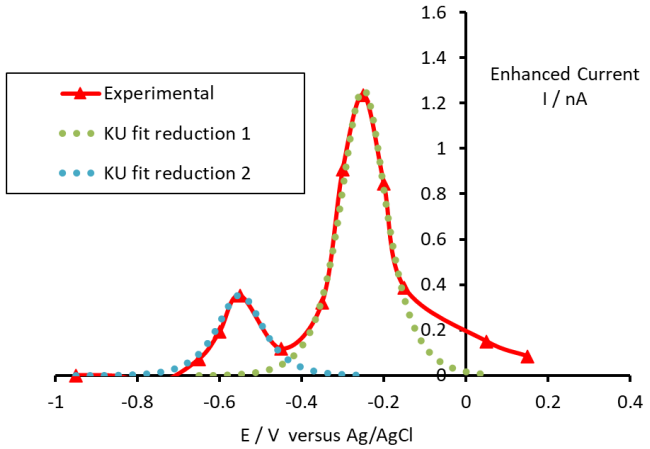

Figure 4: Enhanced single molecule junction current versus electrode potential for Au|6V6|graphene in BMIM-OTf. The red triangles and line show the experimental data. The green dotted line shows the fit to the KU equation for the first reduction wave, while the blue dotted line shows the fit for the second reduction. Fitting parameters are discussed in the text.

The experimental data can be fitted with reasonable parameters to both the phase coherent DFT model and the 2-step sequential KU model despite the differing fundamental basis of these two contrasting models. This clearly merits further investigations. An obvious suggestion here would be to investigate temperature dependence since the first assumption would be that a coherent tunnelling mechanism would be temperature independent while an incoherent one would exhibit temperature dependence. However, this is not so obviously the case, since even phase coherent transport has been shown to exhibit significant temperature dependence as a result of the temperature dependence of the Fermi distribution function of the electrodes.[58,59] Experimentally measuring the temperature dependence of molecular conductance over a sufficiently wide temperature range *in situ* in electrolytes is also experimentally challenging.

It should also be stressed that both mechanisms examined here involve assumptions. While the phase coherent DFT computations model the molecular charge changes resulting from electrode potential tuning, they do not account for dynamics in the molecular junction, corresponding to either nuclear dynamics or charge state dynamics associated with temporal charging or discharging of the bridge. The KU model also makes assumptions and requires some difficult choices for parameters. This model calculates the current enhancement on moving the electrode potential from values far away from the redox switching potential to potentials close to the reversible potential. It does of course not include an *ab initio* calculation of the "off resonance" junction conductance. An important aspect of this work is that it raises fundamental questions with respect to the definition of the states used to describe the system and the transition mechanisms between these states. Indeed, in the DFT approach, we consider the evolution of the initially defined HOMO and LUMO levels through the charging of the molecule and their corresponding resonances. These levels consist in monoelectronic levels, as described in DFT. Oppositely in the KU approach, we consider a transition between the so-called redox states defined intrinsically, which do not evolve with the electric field. These states can be defined as collective states of the system. Hence, in one case we consider the evolution of monoelectronic resonances with the electric field, while in the other we consider a transition induced by the electric field between well-established collective states. Both models of course do not consider that there might be contributions from both mechanisms operating simultaneously under the given operating conditions. Computational modelling which could reasonably account for all of these factors would be indeed very challenging and will have to wait for future step-changes in methodology.

From an experimental viewpoint, characterization of junction nuclear or charge dynamics is well beyond any reasonably achievable experimental determination. Nevertheless, it is noted recently that long lived "trapped" charged states have been identified in redox active molecular junctions. Such long lived charge states have been detected in Au-viologen-Au nanoparticle on mirror (NPoM) junctions.[60] Here, time resolved Raman spectra followed the dynamics of temporary populated charged states of these molecular junctions which could be spectroscopically tracked in real time. In these experiments, the transient charge states were created by plasmon-induced hot electron transfer between gold nanoparticles and the LUMO of the viologen.[59] Unexpectedly long-lived charge states have also been detected in single molecule Au|oligo-porphyrin|Au molecular junctions by rapidly recording I-V traces.[61] Such long-lived charge states were formed in these 2-terminal junctions for moderate junction bias voltages (~1 V). The longevity of such transient charged junction states greatly exceeds the expected relaxation dynamics associated with reorganization and relaxation at the redox centre, prior to and following the electron transfer steps in the KU model. Nevertheless, the possible role of unusually long-lived ("trapped") charge states should also be further investigated to see if they may be playing a role under electrochemical conditions in nanoscale junctions. If they are playing a role then a fundamental re-evaluation of mechanisms for charge transfer in such redox active nano-electrical junctions will be needed.

Conclusions

To summarize, we have studied here the electrical conductance of viologen based molecular junctions using gold and graphene heterojunction electrodes contacts. Using an electrochemical STM, with a gold STM tip and graphene substrate, the single molecule conductance has been measured as a function of the electrochemical gating potential applied in the ionic liquid, 1-butyl-3-methylimidazolium triflate (BMIM-OTf). An efficient

electrochemical gate tuning of the conductance of Au|6V6|graphene junctions is achieved, which is characterised by a clear and sharp peak in the single molecule conductance versus electrochemical potential data for the first reduction wave of the viologen. The peak conductance at this first reduction wave of Au|6V6|graphene molecular junctions (5.9 nS) is nearly four times larger than that of previously measured Au|6V6|Au junctions (1.5 nS) in ionic liquid. This might be attributed to the weak coupling at the molecule/graphene interface, leading to a sharp molecular resonance. The impact of the second reduction step of the viologen to its neutral form on the molecular conductance is also observed for the first time. The second reduction wave gives a smaller molecular conductance enhancement than the first wave.

We compare these data with two theoretical models, namely first principles density functional theory (DFT) calculations and the Kuznetsov Ulstrup sequential electron transfer model. Both models, despite their very different physical origin can be fitted to the experimental data within reasonable parameter assumptions. DFT is able to simulate the experimental data with a simple gating model in a monoelectronic approach, namely by adding an external potential that shifts the molecular electronic levels and modifies the charge state of the molecule (similarly to the gate in a transistor), which allows accurate identification of the molecular electronic resonances observed. Moreover, comparison with Au|6V6|Au junctions reveals a quantitatively similar behaviour, although peak single molecule conductance values are significantly higher for Au|6V6|graphene junctions. Nevertheless, the qualitatively similar behaviour can be accredited to the active molecular part being decoupled from the electrodes through the alkyl spacer chains. On the other hand, the conductance-overpotential curves can also be fitted to the Kuznetsov Ulstrup sequential electron transfer model within a collective approach, to give reasonable parametric fits. Since both models rely on very different physical mechanisms, it is possible that fitting to either one might be coincidental or that both mechanisms operate under these conditions. Possible future strategies that might help to distinguish the dominant mechanism are discussed. Finally, it is noted that coherent tunnelling (modelled with DFT computations here) and the sequential electron transfer (KU) models are divergent mechanisms. In this sense, it is not feasible to have compliance both, and this is not the intention of this study. The point that we are making is that we can fit data to both models with parameters which are not unreasonable, which means that the charge transport mechanisms for such systems remains open for further investigations. By comparing to, and achieving apparently reasonable fits to both models, we are presenting a challenge to the community to compare fits to divergent models and hopefully then discover future ways, experimental or theoretical, to distinguish between them in such systems.

Data availability

All the experimental procedures, characterization data, as well as the conductance data of Au|6V6|Au, fitting parameters to the Kuznetsov Ulstrup Model, DFT calculated isoelectronic density of states supporting this article have been uploaded as part of the ESI.†

Author Contributions

L. Y., R. J. N., and C. Z. Z. designed experiments; S.T. carried out experiments on the conductance measurement, data analysis and wrote the first draft of the manuscript.; A. V. and S. J. H. synthesized the first batch of the 6V6 molecule; Q. Z. and C. Z. helped to discuss the experimental results. A. S. and Y. J. D. conducted the simulation work and developed analysis tools. L. Y., Y. J. D. and R. J. N. wrote the model part and completed the manuscript. All authors have given approval to the final version of the manuscript.

Conflicts of interest

There are no conflicts of interest to declare.

Acknowledgements

This work was supported by the National Natural Science Foundation of China (NSFC Grants 21503169), Suzhou Industrial Park Initiative Platform Development for Suzhou Municipal Key Lab for New Energy Technology (RR0140), Key Program Special Fund in XJTLU (KSF-E-28) and the XJTLU Research Development Fund (RDF-14-02-42, RDF-16-01-33 and REF-19-01-05).

Notes and references

1 W. Haiss, H. van Zalinge, S. J. Higgins, D. Bethell, H. Hobenreich, D. J. Schiffrin, and R. J. Nichols, *J. Am. Chem. Soc.*, 2003, **125**, 15294-15295.
2 W. Haiss, H. van Zalinge, H. Hobenreich, D. Bethell, D. J. Schiffrin, S. J. Higgins, and R. J. Nichols, *Langmuir,* 2004, **20**, 7694-7702.
3 Z. Li, B. Han, G. Meszaros, I. Pobelov, T. Wandlowski, A. Blaszczyk, and M. Mayor, *Faraday Discuss.,* 2006, **131**, 121-143.
4 Z. Li, I. Pobelov, B. Han, T. Wandlowski, A. Blaszczyk, and M. Mayor, *Nanotechnology,* 2007, **18**, 044018.
5 W. Haiss, T. Albrecht, H. van Zalinge, S. J. Higgins, D. Bethell, H. Hoebenreich, D. J. Schiffrin, R. J. Nichols, A. M. Kuznetsov, J. Zhang, Q. Chi, and J. Ulstrup, *J. Phys. Chem. B,* 2007, **111**, 6703-6712.
6 E, Leary, S. J. Higgins, H. van Zalinge, W. Haiss, R. J. Nichols, S. Nygaard, J. Jeppesen, and J. Ulstrup, *J. Am. Chem. Soc.,* 2008, **130**, 12204-12205.
7 I. V. Pobelovt, Z. H. Li, and T. Wandlowski, *J. Am. Chem. Soc.,* 2008, **130**, 16045-16054.
8 B. Han, Z. H. Li; C. Li, I. Pobelov, G. J. Su, R. Aguilar-Sanchez, and T. Wandlowski, *Top. Curr. Chem.*, 2009, Vol. **287**, 181-255.
9 V. Kolivoska, M. Valasek, M. Gal, R. Sokolova, J. Bulickova, L. Pospisil, G. Meszaros, and M. Hromadova, *J. Phys. Chem. Lett.,* 2013, **4**, 589-595.
10 H. M. Osorio, S. Catarelli, P. Cea, J. B. G. Gluyas, F. Hartl, S. J. Higgins, E. Leary, P. J. Low, S. Martin, R. J. Nichols, J. Tory, J. Ulstrup, A. Vezzoli, D. C. Milan, and Q. Zeng, *J. Am. Chem. Soc.,* 2015, **137**, 14319-14328.

11 W. Zhang, S. Gan, A. Vezzoli, R. J. Davidson, D. C. Milan, K. V. Luzyanin, S. J. Higgins, R. J. Nichols, A. Beeby, P. J. Low, B. Li, and L. Niu, *ACS Nano,* 2016, **10**, 5212-5220.
12 N. Darwish, I. Diez-Perez, P. Da Silva, N. J. Tao, J. J. Gooding, and M. N. Paddon-Row, *Angew. Chem. Int. Ed.,* 2012, **51**, 3203-3206.
13 N. Darwish, I. Diez-Perez, S. Y. Guo, N. J. Tao, J. J. Gooding, and M. N. Paddon-Row, *J. Phys. Chem. C,* 2012, **116,** 21093-21097.
14 M. Baghernejad, X. T. Zhao, K. B. Ornso, M. Fueg, P. Moreno-Garcia, A. V. Rudnev, V. Kaliginedi, S. Vesztergom, C. C. Huang, W. J. Hong, P. Broekmann, T. Wandlowski, K. S. Thygesen, and M. R. Bryce, *J. Am. Chem. Soc.,* 2014, **136**, 17922-17925.
15 Z. Li, H. Li, S. Chen, T. Froehlich, C. Yi, C. Schoenenberger, M. Calame, S. Decurtins, S. X. Liu, and E. Borguet, *J. Am. Chem. Soc.,* 2014, **136**, 8867-8870.
16 J. Bai, A. Daaoub, S. Sangtarash, X. Li, Y. Tang, Q. Zou, H. Sadeghi, S. Liu, X. Huang, Z. Tan, J. Liu, Y. Yang, J. Shi, G. Mészáros, W. Chen, C. Lambert, and W. Hong, *Nat. Mater.,* 2019, **18**, 364-369.
17 H. X. He, X. L. Li, N. J. Tao, L. A. Nagahara, I. Amlani, and R. Tsui, *Phys. Rev. B,* 2003, **68**, 045302.
18 F. Chen, J. He, C. Nuckolls, T. Roberts, J. E. Klare, and S. Lindsay, *Nano Lett.,* 2005, **5,** 503-506.
19 B. Q. Xu, X. L. Li, X. Y. Xiao, H. Sakaguchi, N. J. Tao, *Nano Lett.,* 2005, **5**, 1491-1495.
20 I. Visoly-Fisher, K. Daie, Y. Terazono, C. Herrero, F. Fungo, L. Otero, E. Durantini, J. J. Silber, L. Sereno, D. Gust, T. A. Moore, A. L. Moore, and S. M. Lindsay, *Proc. Natl. Acad. Sci. U.S.A.,* 2006, **103**, 8686-8690.
21 J. He, F. Chen, S. Lindsay, and C. Nuckolls, *Appl. Phys. Lett.,* 2007, **90**, 072112.
22 X. Y. Xiao, D. Brune, and J. He, *Chem. Phys.,* 2006, **326**, 138-143.
23 S. Chappell, C. Brooke, R. J. Nichols, L. J. Kershaw Cook, M. Halcrow, J. Ulstrup, and S. J. Higgins*, Faraday Discuss.,* 2016, **193**, 113-131.
24 Y. Q. Li, H. Wang, Z. X. Wang, Y. J. Qiao, J. Ulstrup, H. Y. Chen, G. Zhou, and N. J. Tao, *Proc. Natl. Acad. Sci. U.S.A.,* 2019, **116**, 3407-3412.
25 X. L. Li, B. Q. Xu, X. Y. Xiao, X. M. Yang, L. Zang, and N. J. Tao, *Faraday Discuss.*, 2006, **131**, 111-120.
26 B. Q. Xu, X. Y. Xiao, X. M. Yang, L. Zang, and N. J. Tao, *J. Am. Chem. Soc.,* 2005, **127**, 2386-2387.
27 X. L. Li, J. Hihath, F. Chen, T. Masuda, L. Zang, and N. J. Tao, *J. Am. Chem. Soc.,* 2007, **129**, 11535-11542.
28 C. Li, A. Mishchenko, Z. Li, I. Pobelov, T. Wandlowski, X. Q. Li, F. Wuerthner, A. Bagrets, and F. Evers, *J. Phys. Condens. Matter,* 2008, **20**, 374122.
29 I. Diez-Perez, Z. Li, S. Guo, C. Madden, H. Huang, Y. Che, X. Yang, L. Zang, and. N. J. Tao, *ACS Nano,* 2012, **6**, 7044-7052.
30 C. Li, V. Stepanenko, M. J. Lin, W. Hong, F. Wuerthner, and T. Wandlowski, *Phys. Status Solidi B*, 2013, **250**, 2458-2467.
31 Y. H. Li, M. Baghernejad, A. G. Qusiy, D. Z. Manrique, G. X. Zhang, J. Hamill, Y. C. Fu, P. Broekmann, W. J. Hong, T. Wandlowski, D. Q. Zhang, and C. Lambert, *Angew. Chem. Int. Ed.,* 2015, **54**, 13586-13589.
32 S. Hosseini, C. Madden, J. Hihath, S. Y. Guo, L. Zang, and Z. H. Li, *J. Phys. Chem. C,* 2016, **120**, 22646-22654.
33 J. Zhang, A. M. Kuznetsov, I. G. Medvedev, Q. Chi, T. Albrecht, P. S. Jensen, and J. Ulstrup, *Chem. Rev.,* 2008, **108**, 2737-2791.
34 A. M. Kuznetsov, and J. Ulstrup, *J. Phys. Chem. A*, 2000, **104**, 11531–11540.
35 M. Kiguchi, S. Miura, T. Takahashi, K. Hara, M. Sawamura, and K. Murakoshi, *J. Phys. Chem. C,* 2008, **112**, 13349-13352.
36 K. Yokota, M. Taniguchi, and T. Kawai, *J. Phys. Chem. C,* 2010, **114**, 4044-4050.
37 S. Ahn, S. V. Aradhya, R. S. Klausen, B. Capozzi, X. Roy, M. L. Steigerwald, C. Nuckolls, and L. Venkataraman, *Phys. Chem. Chem. Phys.,* 2012, **14**, 13841-13845.
38 R. J. Brooke, C. Jin, D. S. Szumski, R. J. Nichols, B. W. Mao, K. S. Thygesen, and W. Schwarzacher, *Nano Lett.,* 2015, **15**, 275-280.
39 C. Fang, Z. Huang, and N. J. Tao, *Appl. Phys. Lett.,* 2007, **91**, 277-245.
40 X. F. Guo, J. P. Small, J. E. Klare, Y. L. Wang, M. S. Purewal, I. M. Tam, B. H. Hong, R. Caldwell, L. M. Huang, S. O'Brien, J. M. Yan, R. Breslow, S. J. Wind, J. Hone, P. Kim, and C. Nuckolls, *Science,* 2006, **311**, 356-359.
41 Q, Zhang, S. Tao, R. Yi, C. He, C. Zhao, W. Su, A. Smogunov, Y. J. Dappe, R. J. Nichols, and L. Yang, *J. Phys. Chem. Lett.,* 2017, **8**, 5987-5992.
42 Q. Zhang, L. Liu, S. Tao, C. Wang, C. Zhao, C. Gonzalez, Y. J. Dappe, R. J. Nichols, and L. Yang, *Nano Lett.,* 2016, **16**, 6534-6540.
43 L. Liu, Q. Zhang, S. Tao, C. Zhao, E. Almutib, Q. Galiby, S. W. D. Bailey, L. Grace, C. J. Lambert, J. Du, and L. Yang, *Nanoscale,* 2016, **8**, 14507-14513.
44 T. Kim, Z. Liu, C. Lee, J. B. Neaton, and L. Venkataraman, *Proc. Natl. Acad. Sci. U. S. A.,* 2014, **111**, 10928-10932.
45 A. Vezzoli, R. J. Brooke, N. Ferri, S. J. Higgins, W. Schwarzacher, and R. J. Nichols, *Nano Lett.,* 2017, **17**, 1109-1115.
46 A. Vezzoli, R. J. Brooke, S. J. Higgins, W. Schwarzacher, and R. J. Nichols, *Nano Lett.,* 2017, **17**, 6702-6707.
47 A. C. Aragones, N. Darwish, S. Ciampi, F. Sanz, J. J. Gooding, and I. Diez-Perez, *Nat. Commun.,* 2017, **8**, 15056.
48 T. Albrecht, K. Moth-Poulsen, J. B. Christensen, J. Hjelm, T. Bjornholm, and J. Ulstrup, *J. Am. Chem. Soc.,* 2006, **128**, 6574-6575.
49 N. J. Kay, R. J. Nichols, S. J. Higgins, W. Haiss, G. Sedghi, W. Schwarzacher, and B. W. Mao, *J. Phys. Chem. C,* 2011, **115**, 21402-21408.
50 N. J. Kay, S. J. Higgins, J. O. Jeppesen, E. Leary, J. Lycoops, J. Ulstrup, and R. J. Nichols, *J. Am. Chem. Soc.,* 2012, **134**, 16817-16826.
51 S. R. Catarelli, S. J. Higgins, W. Schwarzacher, B. W. Mao, J. W. Yan, and R. J. Nichols, *Langmuir,* 2014, **30**, 14329-14336.
52 C. L. Wu, X. H. Qiao, C. M. Robertson, S. J. Higgins, C. X. Cai, R. J. Nichols, and A. Vezzoli, *Angew. Chem. Int. Ed.,* 2020, **59**, 12029-12034.
53 M. Armand, F. Endres, D. R. Macfarlane, H. Ohno, and B. Scrosati, *Nat. Mater.,* 2009, **8**, 621.
54 J. G. Huddleston, A. E. Visser, W. M. Reichert, H. D. Willauer, G. A. Broker, and R. D. Rogers, *Green Chem.,* 2001, **3**, 156-164.
55 E. I. Rogers, B. Šljukić, C. Hardacre, R. G. Compton, *J. Chem. Eng. Data,* 2009, **54**, 2049-2053.
56 A. P. Abbott, and K. J. McKenzie, *Phys. Chem. Chem. Phys.,* 2006, **8**, 4265–4279.
57 X. D. Yin, Y. P. Zang, L. L. Zhu, J. Low, Z. F. Liu, J. B. Neaton, L. Venkataraman, L. M. Campos, Sci. Adv., 2017, 3, eaao2615.
58 S. Snegir, Y. J. Dappe, D. Sysoiev, O. Pluchery, T. Huhn, E. Scheer, *Phys. Chem. Chem. Phys.,* 2021, **23**, 9930–9937.
59 D. Di Felice, Y. J. Dappe, *Nanotech.* 2018, **29**, 505708.
60 R. Harsh, F. Joucken, C. Chacon, V. Repain, Y. Girard, A. Bellec, S. Rousset, R. Sporken, A. Smogunov, Y. J. Dappe, J. Lagoute, *J. Phys. Chem. Lett.,* 2019, **10**, 6897-6903.
61 T. Albrecht, A. Guckian, A. M. Kuznetsov, J. G. Vos, J. Ulstrup, *J. Am. Chem. Soc.,* 2006, **128**, 17132-17138.
62 W. Haiss, T. Albrecht, H. van Zalinge, S. J. Higgins, D. Bethell, H. Hoebenreich, D. J. Schiffrin, R. J. Nichols, A. M. Kuznetsov,

J. Zhang, Q. Chi, J. Ulstrup, *J. Phys. Chem. B,* 2007, **111**, 6703-6712.
63 G. Sedghi, V. M. Garcia-Suarez, L. J. Esdaile, H. L. Anderson, C. J. Lambert, S. Martin, D. Bethell, S. J. Higgins, M. Elliott, N. Bennett, J. E. Macdonald, and R. J. Nichols, *Nat. Nanotechnol.,* 2011, **6**, 517-523.
64 M. Poot, E. Osorio, K. O'Neill, J. M. Thijssen, D. Vanmaekelbergh, C. A. van Walree, L. W. Jenneskens, and H. S. J. van der Zant, *Nano Lett.,* 2006, **6**, 1031-1035.
65 B. de Nijs, F. Benz, S. J. Barrow, D. O. Sigle, R. Chikkaraddy, A. Palma, C. Carnegie, M. Kamp, R. Sundararaman, P. Narang, O. A. Scherman, and J. J. Baumberg, *Nat. Commun.,* 2017, **8**, 994.
66 E. Leary, G. Kastlunger, B. Limburg, L. Rincon-Garcia, J. Hurtado-Gallego, M. T. Gonzalez, G. R. Bollinger, N. Agrait, S. J. Higgins, H. L. Anderson, R. Stadler, and R. J. Nichols, R. J. *Nanoscale Horiz.,* 2021, **6**, 49-58.